MATERIALS SCIENCE

Heat conduction tuning by wave nature of phonons

Jeremie Maire,[1,2]* Roman Anufriev,[1] Ryoto Yanagisawa,[1] Aymeric Ramiere,[1,2] Sebastian Volz,[3] Masahiro Nomura[1,4,5]*

The world communicates to our senses of vision, hearing, and touch in the language of waves, because light, sound, and even heat essentially consist of microscopic vibrations of different media. The wave nature of light and sound has been extensively investigated over the past century and is now widely used in modern technology. However, the wave nature of heat has been the subject of mostly theoretical studies because its experimental demonstration, let alone practical use, remains challenging due to its extremely short wavelengths. We show a possibility to use the wave nature of heat for thermal conductivity tuning via spatial short-range order in phononic crystal nanostructures. Our experimental and theoretical results suggest that interference of thermal phonons occurs in strictly periodic nanostructures and slows the propagation of heat. This finding expands the methodology of heat transfer engineering to the wave nature of heat.

INTRODUCTION

Interference—one of the most remarkable wave phenomenon—can be demonstrated in periodic structures, where systematic reflections of waves result in their constructive and destructive interference. Specifically designed periodic structures can even fully control the propagation of light (photons) or sound (phonons) and thus are called photonic (*1*, *2*) or phononic crystals (*3*, *4*). However, the application of this concept to manipulation of heat (ensemble of thermal phonons) requires nanoscale periodicity and exceptionally smooth interfaces (*5*). Wavelengths of thermal phonons at room temperature are only a few nanometers (*6*, *7*), and phonons quickly lose their phase (coherence), being scattered at surfaces with nanometer-scale roughness (*8*). For this reason, room temperature coherent scattering of thermal phonons (that is, scattering with preserved phase) has been demonstrated only in superlattices with atomically smooth interfaces and nanometer-size periodicity (*9*, *10*). However, many of the practical applications of this phenomenon, such as waveguides or cloaking, cannot be realized in superlattices and require two-dimensional (2D) structures (*11*), similar to those used in photonics to manipulate light (*1*, *2*). These 2D phononic crystals can be fabricated via lithography techniques, but the atomically smooth surfaces and short periodicity are challenging to achieve.

In the past decade, advances in nanofabrication (*12*) resulted in a burst of experimental demonstrations of the reduction in thermal conductivity of 2D phononic crystal structures, which was attributed to the interference of thermal phonons (*13*–*15*). But some theoretical works (*7*, *16*, *17*) recognized that this reduction originates from factors unrelated to phonon interference (for example, surface roughness and strong surface scattering). Thus, the low absolute value of thermal conductivity alone cannot be an indication of phonon interference, and comparative studies are required to detect the precise impact of this phenomenon.

Moreover, the periodicity is typically set for a specific and rather long wavelength, but, unlike light or sound, heat essentially consists of thermal phonons in a broad range of rather short wavelengths (*7*). Nevertheless, recent theoretical studies on 2D phononic crystals have demonstrated that phonon interference, due to periodicity of holes (*18*, *19*) or local resonances in pillars (*20*–*22*), can actually affect the entire phonon spectrum, reducing overall phonon group velocity and density of states, whereas experiments at sub-kelvin temperatures have shown that, if phonon wavelengths are sufficiently long, thermal conductance can be fully controlled by phonon interference, despite the micrometer scale of the phononic crystals (*18*, *23*). Recently, Wagner *et al.* (*24*) showed that although low-frequency phonon modes are affected by periodicity, their impact is not sufficient to affect thermal conductivity at room temperature (*24*, *25*). In addition, the modified dispersion of low-frequency modes has been demonstrated in thin films (*26*), nanowires (*26*–*28*) and nanoporous nanostructures (*29*), and their impact on heat conduction is discussed. Hence, the wide gap between ultralow temperatures and room temperature remains unexplored despite the attractiveness of thermal conductivity tuning using periodic nanostructures.

Here, we demonstrate this tuning of thermal conductivity in 1D and 2D phononic crystal nanostructures. We show that the presence of phonon interference reduces thermal conductivity of phononic crystal with an ordered array of holes as compared to the thermal conductivity of structures with randomly positioned holes. The temperature dependence of this effect displays the transition from coherent to incoherent heat transport regime, thus answering the long-lasting question about the working range of phononic crystals. In addition, we perform finite element method (FEM) and Monte Carlo simulations to show that our observations cannot be attributed to incoherent scattering mechanisms. Finally, we propose a phenomenological model that takes into account both coherent and incoherent phonon scattering mechanisms to explain our experimental data.

RESULTS

Fabrication and measurements

We study phononic crystals with 1D (Fig. 1A) and 2D (Fig. 1B) arrays of holes. All samples were fabricated on a silicon-on-insulator (SOI) wafer with a 145-nm-thick single-crystalline top silicon layer (Methods). Each sample consisted of a suspended 5 μm × 5 μm silicon island topped by a 4 μm × 4 μm aluminum pad and supported by five nanobeams (0.3 μm × 10 μm) or a membrane (5 μm × 15 μm) on each side. The phononic crystals, with a period of 300 nm, were formed in the nanobeams and membranes and consisted of arrays of holes with

[1]Institute of Industrial Science, University of Tokyo, Tokyo 153-8505, Japan. [2]Laboratory for Integrated Micro Mechatronic Systems/National Center for Scientific Research–Institute of Industrial Science, University of Tokyo, Tokyo 153-8505, Japan. [3]Laboratoire d'Energétique Moléculaire et Macroscopique, Combustion, UPR CNRS 288, Ecole Centrale Paris, Grande Voie des Vignes, F-92295 Châtenay-Malabry, France. [4]Institute for Nano Quantum Information Electronics, University of Tokyo, Tokyo 153-8505, Japan. [5]PRESTO, Japan Science and Technology Agency, Saitama 332-0012, Japan.
*Corresponding author. Email: nomura@iis.u-tokyo.ac.jp (M.N.); jmaire@iis.u-tokyo.ac.jp (J.M.)

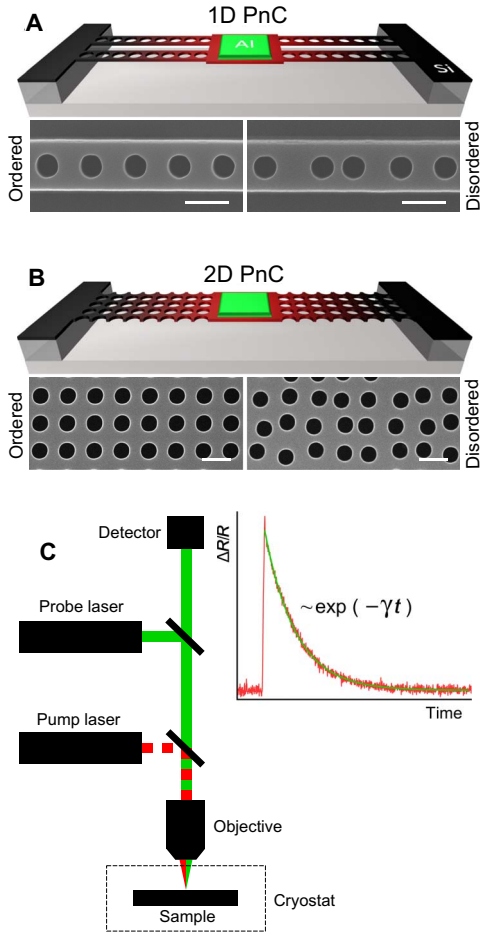

Fig. 1. Samples and experimental setup. Schematic and SEM images show fabricated samples of 1D (**A**) and 2D (**B**) phononic crystals (PnC) with ordered (δ = 0%) and disordered (δ = 15%) arrays of holes. Scale bars, 300 nm. (**C**) Schematic of the micro-TDTR setup, with inset showing a typical thermal decay curve with an exponential fitting.

diameters of 161 and 133 nm in 1D and 2D phononic crystals, respectively. A set of samples consisted of the structures with degrees of disorder (δ) in the range of 0 to 14% (Fig. 1), where the shift of each hole from its aligned position is given by ε·δ·300 nm, with ε as a random number in the range of −1 to +1. Because each set of samples was fabricated simultaneously on the same wafer, the surface roughness did not vary from one sample to another. Surface roughness of the top and bottom surfaces is negligible (*30*) compared to that of the other surfaces, whose roughness was estimated to be in the range of 1 to 3 nm (Methods) (*30*, *31*).

To study the in-plane heat conduction in the phononic crystals, we used a micro-TDTR (time-domain thermoreflectance) technique (*32*), originally designed for suspended micrometer-sized membranes (Methods). The schematic of the experimental setup is shown in Fig. 1C. The samples are mounted in a He flow cryostat. A pulse laser beam (642 nm) periodically heats the aluminum pad in the center of the sample, whereas a continuous laser beam (785 nm) constantly measures the relative change of its reflectivity ($\Delta R/R$) caused by the increase in temperature. Because heat gradually dissipates after each heating pulse, the reflectivity returns to its initial value. The measured time (t) dependence of this heat dissipation (Fig. 1C) can always be well fitted by an exponential decay, $\exp(-\gamma t)$, where γ is the thermal decay rate—the only parameter characterizing heat conduction in each sample. The standard deviation (SD) of the thermal decay rate is calculated from its fluctuations over time and remains less than 2%.

Impact of disorder on thermal transport

First, we investigate the impact of the disorder on heat conduction in phononic crystals at the temperature of 4 K (Fig. 2). In the samples with significantly disordered positions of holes (δ > 5%), heat dissipates at the same rate, regardless of the disorder degree. But in the samples with small disorder degrees (δ < 5%), heat dissipation slows down, becoming 8.5 and 19% slower in perfectly ordered 1D and 2D phononic crystals, respectively. In terms of thermal conductivity, the reduction in ordered structures reaches 8.5 and 21%, respectively (fig. S4); thus, the short-range order of the phononic crystal can be used to tune the thermal conductivity of nanostructures.

At room temperature, however, this reduction is absent and the decay rates seem to be independent of the disorder (insets of Fig. 2), with average thermal conductivities of 33 W m^{-1} K^{-1} for 1D and 42 W m^{-1} K^{-1} for 2D phononic crystals. We performed FEM simulations based on the Fourier heat transport equation, keeping all parameters, except the disorder degree, identical (fig. S5). The results, displayed as solid lines in Fig. 2, show no impact of disorder in the Fourier heat transport limit.

To show that incoherent scattering mechanisms cannot explain the experimental results, we also performed 2D Monte Carlo simulations of phonon transport in our samples (fig. S6). These simulations take into account impurity, boundary, and phonon-phonon scattering but not the phonon interference. The simulations show no impact of disorder for 1D phononic crystals, whereas periodic structures transmit heat more efficiently in the case of 2D phononic crystals, contrary to our experimental observations. This phenomenon observed from Monte Carlo simulations stems from holes obstructing otherwise free phonon passages as disorder increases (*30*). Thus, only coherent phonon scattering remains to explain the experimental results.

To explain these results, we elaborate a phenomenological model in which the phonon spectrum is divided into coherent and incoherent parts according to the degree of disorder and temperature. Recently, Wagner *et al.* (*24*) experimentally demonstrated that coherent phonon modes could exist up to 50 GHz in their ordered 2D phononic crystals but only up to 20 GHz in the disordered one. The cutoff frequency, below which all modes are interfering coherently, was empirically determined in phononic crystals with a period of 300 nm as $f_c(R) = 0.0493\ v_L/R$, where $v_L = 8433$ m s^{-1} is the frequency-independent longitudinal sound velocity in silicon (*24*, *33*), and R is an interference dampener parameter. This interference dampener parameter depends on the effective surface roughness, which reduces the coherence, and the average displacement of the holes from their ordered position ($\xi = 0.5 \cdot \delta \cdot 300$ nm), which blurs the interference pattern. We calculate R as $(\sigma_{eff}^{\ 2} + (0.5\xi)^2)^{1/2}$, where $\sigma_{eff} \approx 2$ nm for 1D and $\sigma_{eff} \approx 1.5$ nm for 2D phononic crystals. For example, for our ordered 1D structure (that is, $R = 2$ nm), this approach yields a cutoff frequency of $f_c = 208$ GHz.

Because coherent modifications of the phonon dispersion markedly suppress thermal conductance in phononic crystals (fig. S7) due to the reduction of both the group velocity and density of states in the entire frequency spectrum (*18*, *19*), we can assume that phonons below the cutoff frequency contribute very little to the heat conduction and heat is carried mostly by phonons above the cutoff frequency. The part of phonon spectrum above the cutoff frequency can be approximated by the Planck distribution for phonons. As disorder is introduced,

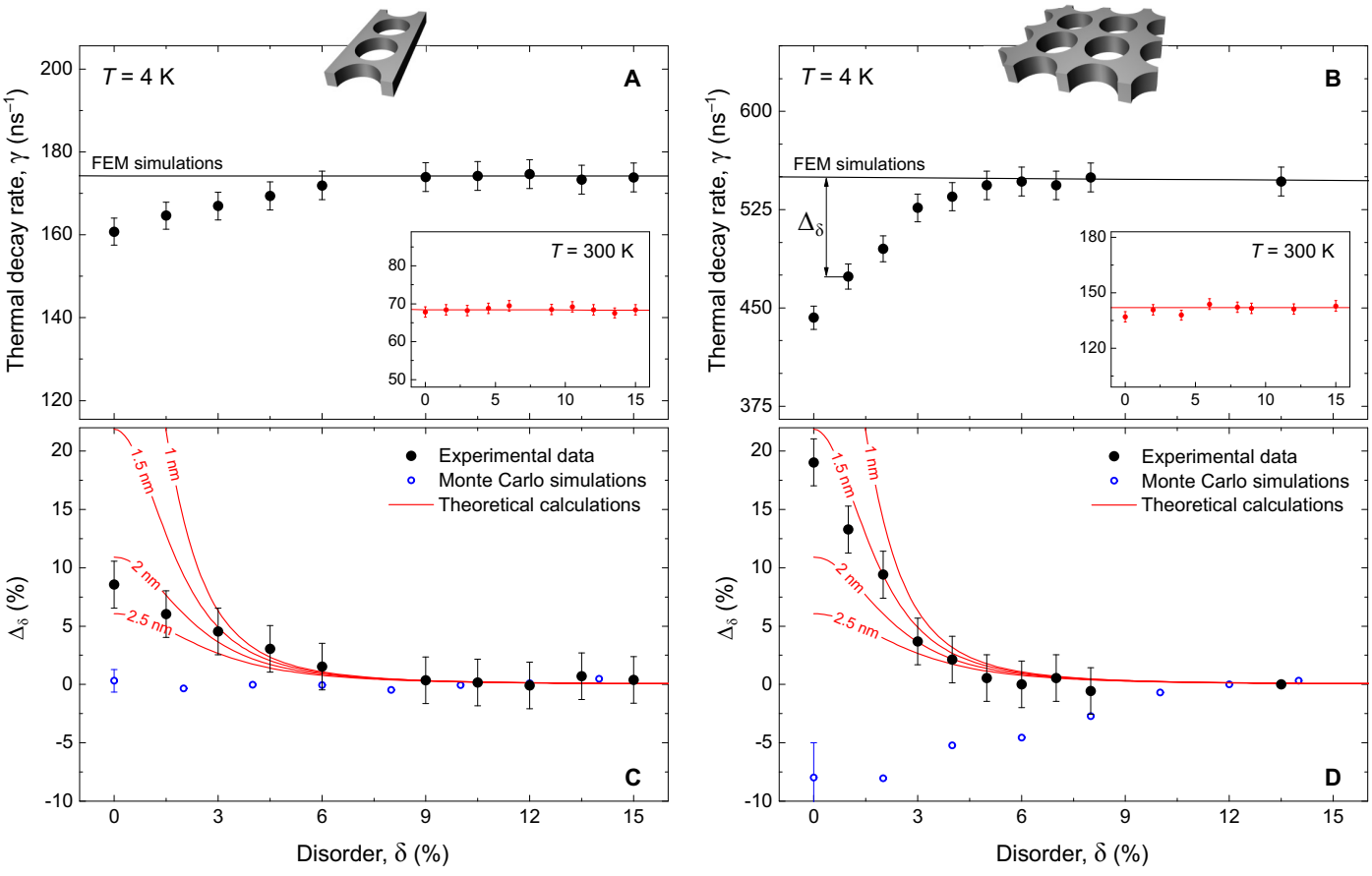

Fig. 2. Thermal decay rate measurements with varying disorder. Measured thermal decay rates in both (**A**) 1D and (**B**) 2D ordered phononic crystals deviate from those in disordered structures at 4 K, whereas at 300 K (insets) heat dissipates through ordered and disordered structures at an equal rate. Error bars show an SD during the measurements (also included in the points at 300 K). Solid lines show results of the FEM simulations based on the Fourier heat transport equation. (**C** and **D**) Theoretically expected disorder dependence alongside the experimentally measured difference between thermal decay rates [$\Delta_\delta = (\gamma_{disordered} - \gamma_\delta)/\gamma_{disordered}$] for 1D and 2D phononic crystals, respectively. The values of effective surface roughness used in the theoretical model are displayed on the corresponding fits. Disorder dependence of the difference Δ_δ in the Monte Carlo simulations (blue scatters). The inaccuracy of Monte Carlo simulation data was estimated as an SD in multiple simulations of the same structure and is equal to 1 and 2.5% for (C) and (D), respectively.

the cutoff frequency shifts to lower frequencies and more phonons become propagating, thus increasing the thermal conductance.

Then, the experimentally measured difference between ordered and strongly disordered structures, calculated as $\Delta_0 = (\gamma_{disordered} - \gamma_{ordered})/\gamma_{disordered}$, is equal to the ratio of the phonon spectrum below the cutoff frequency to the entire spectrum The value of the difference for a given amount of disorder, characterized by a cutoff frequency $f_c(R)$, is thus calculated as

$$\Delta = \frac{\int_0^{f_c(R)} Q(f)df}{\int_0^{\infty} Q(f)df} \quad (1)$$

where Q is the heat flux spectrum (fig. S9 and derivation in section S7). Figure 2 (C and D) shows that this model, using the effective surface roughness as a fitting parameter, quantitatively agrees with the experimental data for both 1D and 2D phononic crystals: Δ is about 9 and 21% in the ordered structures and gradually decreases with disorder due to the reduction of the cutoff frequency. Above 6% disorder, the effect becomes negligible, as the portion of coherent phonons becomes negligible to significantly affect heat conduction. The difference in effective surface roughness between 1D and 2D phononic crystals stems from the impact of the sidewalls of the beam, which have a larger roughness than the holes (Fig. 1A). This results in a lower effective roughness in 2D phononic crystals (Fig. 2, C and D). However, the stronger effect in 2D phononic crystals can also result from higher symmetry of 2D structures as compared to 1D ones. Therefore, we suggest that 3D phononic crystals may be even more efficient in suppressing heat conduction due to even higher symmetry and thus stronger modifications of the phonon dispersion (*34*).

Impact of temperature for 1D phononic crystals

Because the difference between strictly periodic structures and highly disordered ones appears at 4 K but not at 300 K, we investigate the temperature dependence in more detail, focusing on the 1D phononic crystals for simplicity. Figure 3 shows the temperature dependence of the difference between the decay rates in the phononic crystals with perfectly aligned (δ = 0%) and disordered arrays of holes (average between structures with δ = 10.5 and 12%). We see a gradual decrease from the value of 8.5%, observed at 4 K, toward the absence of difference, as was observed at 300 K. These experimental results imply that phonon interference occurs in the ordered phononic crystals only at low temperatures,

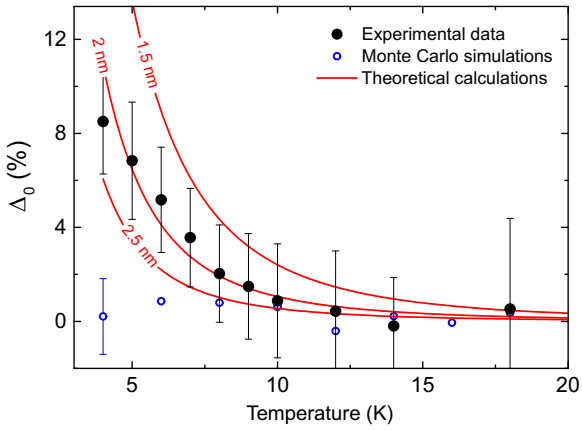

Fig. 3. Comparison between experiment and theories. Temperature dependence of the difference between thermal decay rates, calculated as $\Delta_0 = (\gamma_{disordered} - \gamma_{ordered})/\gamma_{disordered}$, obtained experimentally and predicted by Monte Carlo simulations and the theory of cutoff frequency for different values of effective surface roughness. Error bars show an upper bound of the signal deviation during the measurement. The inaccuracy of the Monte Carlo simulation data is lower than 2% for all points.

where the phonon wavelengths can reach tens of nanometers, enabling coherent reflections of thermal phonons. As temperature is increased, however, the range of phonon wavelengths shortens from 10 to 100 nm at 4 K to 0.5 to 6 nm (*6*, *35*, *36*) at room temperature. Thus, as temperature is increased, the effect disappears because the coherent part of the phonon spectrum becomes negligible even in the ordered structure. Because the weakening of the effect with temperature is closely related to the length of phonon wavelengths as compared to surface roughness, we do not expect this effect to be present at higher temperatures in 2D or even in 3D structures with the same surface roughness.

Next, we compare the temperature dependence obtained experimentally to that expected from our model. Figure 3 shows that the theoretical curve with an effective roughness of 2 nm, consistent with the roughness of the fabricated structures (Fig. 4), is again in good agreement with our experimental data. At temperatures above 4 K, the phonon population shifts to frequencies of hundreds of gigahertz, and the reduction in thermal conductance due to the coherent phonon modes below 208 GHz no longer significantly affects the total heat conduction. For this reason, we observed the weakening of the effect as temperature increases, and finally detected nearly no impact of the disorder on the thermal conductivity above 10 K, in agreement with estimations by Marconnet *et al.* (*37*). The absence of impact of disorder stays all the more valid at room temperature, in agreement with Wagner *et al.* (*24*) and Lee *et al.* (*25*).

DISCUSSION

Our experimental data showed that heat conduction can be tuned using the wave nature of phonons; interference hinders phonon propagation in phononic crystals. Hence, a decrease of disorder yields a reduction in thermal conductivity, whereas in a high disorder state thermal conductivity remains unaffected. Our simulations showed that this effect can be explained only by coherent scattering of phonons. Although our cutoff frequency model does not explain the microscopic physical mechanisms of the observed phenomenon, it successfully corroborates our experimental observations. A more precise theoretical model, describing this intermediate range where both particle and wave regimes have to be considered, must include transient mechanisms, such as a time-dependent phonon distribution, and should be the subject of a future work. However, our findings advance the applicability of phononic crystals. Whereas Zen *et al.* (*18*) and Maasilta *et al.* (*23*) showed coherent reduction of thermal conductance at sub-kelvin temperatures, here we demonstrated thermal conduction control at one-order higher temperatures, until the transition to purely diffusive heat conduction was observed at 10 K. The temperatures at which this effect is observed allow for uses in low-temperature applications, such as detectors and bolometers, or in space. Further miniaturization, the use of materials with longer phonon mean free path such as alloys, and improvements in the hole fabrication process can further enhance the working temperature range, because it has been shown that phonon confinement occurred in smooth nanowires (*28*) and nanoporous arrays of smaller dimensions (*29*) even at room temperature, in agreement with our results here. At higher temperatures, the absolute strength of this effect decreases, but as thermal conductivity is already reduced by incoherent scattering mechanisms, the contribution of coherence becomes relatively larger, all the more so in smaller structures. Thus, we believe that the phononic crystal concept is not bound to only very low temperatures and manipulation of heat transport using the wave nature of phonons is within reach. Further miniaturization will keep broadening the working temperature range of phononic crystals until the expansion of thermal engineering to wave regime completely changes thermal management, in the way that wave optics revolutionized the manipulations of light.

METHODS

Sample fabrication

Each structure was patterned in a region of 20 μm × 40 μm. The structures were prepared on commercially available (100) SOI wafers. The top silicon layer was nominally doped with boron (10^{-15} cm^{-3}), and its thickness was 145 nm. The root mean square (RMS) roughness of the top surface was measured by atomic force microscopy (AFM) and was less than 0.5 nm. The thickness of the buried oxide was 1 μm. On the pattern-free SOI substrate, we spin-coated resist (ZEP520-A7, positive), and 4 μm × 4 μm squares were drawn by electron beam lithography, followed by the development of the resist. A 125-nm-thick aluminum layer was then deposited by electron beam–assisted evaporation before the resist was removed. Immediately afterward, the resist was spin-coated again. All the structures were patterned by electron beam lithography aligned with the previously deposited aluminum pads. The resist was used as a mask for the pattern transfer into the silicon. This step was performed by reactive ion etching (Oxford Instruments Plasmalab System 100) using a mixture of SF_6 and O_2 for 20 s. After the sample cleaning, the buried oxide layer was removed with diluted hydrofluoric acid vapor in a commercial system, which included a heated plate on which the sample was positioned. This etching method provides good control over the etching speed and allows for a stiction-free buried oxide removal. The size parameters of the holes and beams were validated via scanning electron microscopy (SEM).

Surface roughness considerations

We performed high-resolution SEM observations to characterize the surface roughness of our structures. The nominal resolution of the SEM was 0.4 nm. Although it was impossible to accurately measure the surface roughness by SEM, our high-resolution images showed that the peak-to-peak surface irregularity did not exceed 2.5 nm, as

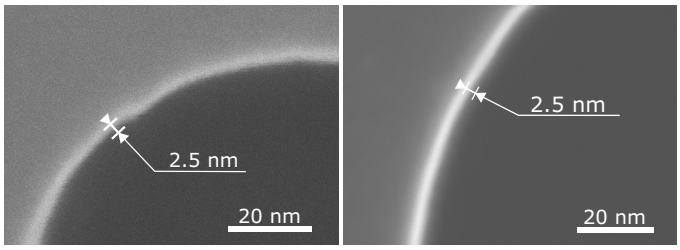

Fig. 4. Hole surface roughness. High-resolution top-view SEM images of two different holes. The surface roughness is contained within a 2.5-nm region. Scale bars, 20 nm.

shown in Fig. 4. The retained value of 2.5 nm for the side walls of the holes was thus an upper bound of the local roughness. Note that the white region visible in the figure did not represent roughness but stemmed from the interaction of the electron beam with the line shape and depended on the acceleration voltage and contrast/brightness.

For the top and bottom surfaces, the maximum surface irregularity, which was larger than the RMS surface roughness, did not exceed 0.5 nm, as characterized by AFM in our previous work (*30*) for identical samples. Hence, the roughness of the top and bottom surfaces can be neglected. The tilted image shown in fig. S3 shows that the profile of the holes is vertical. Although it was challenging to estimate the precise side wall angles from this image, no measurable reduction of diameter was visible. Furthermore, the side walls of the "neck" were parallel to each other, which again showed that we could consider the diameter to be constant over the height of the structure. In addition, surface roughness and hole profiles were identical for all holes, thus not altering our conclusions. Further cross-sectional SEM images on similar samples were taken in our previous work (*30*). See section S2 for the discussion on the impact of the surface roughness and its correlation length on the phonon surface scattering.

Optical measurement

The optical measurement system and the method used to obtain the thermal conductivity were detailed in a previous work (*32*) but were improved to include an automatic exponential fitting of the measurement curve based on the least squares method. The probe laser was a continuous wave laser diode of 785 nm in wavelength. Similarly, the pump was a laser diode (642 nm) but pulsed at the frequency of 1 kHz with pulse durations of 1 μs. Both lasers were focused on the sample, passing through the same 40× microscope objective with an aperture of 0.6. The sample itself was mounted in a He flow cryostat (Oxford Instruments), and measurements were performed under vacuum with a pressure below 10^{-2} Pa at 300 K and 10^{-4} Pa at 4 K to avoid any convection issues. Heat losses through low-pressure gas conduction between the structures and the substrate were less than 1 nW, hence negligible. The temperature increase inside the phononic crystal was estimated by comparing the reflectivity change with values of the thermoreflectance coefficient from the literature (*38*). This increase was estimated to be in the temperature range of 1 to 2 K, and we experimentally verified that the pump power was in a range in which the decay rate did not vary. The input power was typically within the range of 200 to 400 nW. Radiation losses were estimated to be at most 3 nW, which accounted for ~1% of the input power. During measurements at 4 K, the heat load from ambient radiation was approximately 20 nW on a single structure and did not change our conclusions because it did not depend on disorder. After reflection, the intensity of the probe beam was measured by a silicon photodiode with 200-MHz bandwidth connected to an oscilloscope with 1-GHz bandwidth (Tektronix), which performed an average of the signal over 10^4 waveforms. The signal was further box-averaged to improve the signal-to-noise ratio, and its normalized decay was fitted by an exponential decay curve using the least squares methods. The dimensions of the structures were measured by SEM and used to create a FEM model (COMSOL Multiphysics), which virtually reproduced the experiment. The decay times obtained from the simulations for different values of the thermal conductivity were then compared to the experimental decay to extract the measured value of thermal conductivity. The inaccuracy of thermal conductivity measurements was estimated by taking into account the SD on the measurement of the decay rate, the inaccuracies of SEM measurements, and FEM analysis, as explained in detail elsewhere (*39*).

SUPPLEMENTARY MATERIALS

Supplementary material for this article is available at http://advances.sciencemag.org/cgi/content/full/3/8/e1700027/DC1

section S1. Micro-TDTR analysis
section S2. Hole dimensions
section S3. Side wall verticality
section S4. Disorder dependence of thermal conductivity
section S5. FEM simulations
section S6. Monte Carlo simulations
section S7. Calculation of the cutoff frequency for heat flux reduction calculation
fig. S1. Measurement method.
fig. S2. Hole dimensions.
fig. S3. Tilted SEM image of a hole on the side of a membrane.
fig. S4. Thermal conductivities with varying disorder.
fig. S5. FEM simulations.
fig. S6. 2D Monte Carlo map.
fig. S7. Monte Carlo simulation of 1D and 2D disordered structures.
fig. S8. Energy transmission.
fig. S9. Energy density spectra.
fig. S10. Phonon dispersion and heat flux spectra.
fig. S11. Theoretical model: Impact of the specularity parameter.
fig. S12. Theoretical model: Impact of the temperature increase.
table S1. Ranges of hole dimensions for different set of 1D phononic crystals.
References (*40*–*52*)

REFERENCES AND NOTES

1. T. Baba, Slow light in photonic crystals. *Nat. Photonics* **2**, 465–473 (2008).
2. J. D. Joannopoulos, P. Villeneuve, S. Fan, Photonic crystals: Putting a new twist on light. *Nature* **386**, 143–149 (1997).
3. M. Maldovan, Sound and heat revolutions in phononics. *Nature* **503**, 209–217 (2013).
4. E. L. Thomas, T. Gorishnyy, M. Maldovan, Colloidal crystals go hypersonic. *Nat. Mater.* **5**, 773–774 (2006).
5. M. Maldovan, Phonon wave interference and thermal bandgap materials. *Nat. Mater.* **14**, 667–674 (2015).
6. K. Esfarjani, G. Chen, H. T. Stokes, Heat transport in silicon from first-principles calculations. *Phys. Rev. B* **84**, 085204 (2011).
7. N. K. Ravichandran, A. J. Minnich, Coherent and incoherent thermal transport in nanomeshes. *Phys. Rev. B* **89**, 205432 (2014).
8. B. Qiu, G. Chen, Z. Tian, Effects of aperiodicity and roughness on coherent heat conduction in superlattices. *Nanoscale Microscale Thermophys. Eng.* **19**, 272–278 (2016).
9. M. N. Luckyanova, J. Garg, K. Esfarjani, A. Jandl, M. T. Bulsara, A. J. Schmidt, A. J. Minnich, S. Chen, M. S. Dresselhaus, Z. Ren, E. A. Fitzgerald, G. Chen, Coherent phonon heat conduction in superlattices. *Science* **338**, 936–939 (2012).
10. J. Ravichandran, A. K. Yadav, R. Cheaito, P. B. Rossen, A. Soukiassian, S. J. Suresha, J. C. Duda, B. M. Foley, C.-H. Lee, Y. Zhu, A. W. Lichtenberger, J. E. Moore, D. A. Muller, D. G. Schlom, P. E. Hopkins, A. Majumdar, R. Ramesh, M. A. Zurbuchen, Crossover from incoherent to coherent phonon scattering in epitaxial oxide superlattices. *Nat. Mater.* **13**, 168–172 (2014).
11. M. Maldovan, Narrow low-frequency spectrum and heat management by thermocrystals. *Phys. Rev. Lett.* **110**, 25902 (2013).
12. A. M. Marconnet, M. Asheghi, K. E. Goodson, From the casimir limit to phononic crystals: 20 years of phonon transport studies using silicon-on-insulator technology. *J. Heat Transfer* **135**, 061601 (2013).

13. J.-K. Yu, S. Mitrovic, D. Tham, J. Varghese, J. R. Heath, Reduction of thermal conductivity in phononic nanomesh structures. *Nat. Nanotechnol.* **5**, 718–721 (2010).
14. P. E. Hopkins, C. M. Reinke, M. F. Su, R. H. OlssonIII, E. A. Shaner, Z. C. Leseman, J. R. Serrano, L. M. Phinney, I. El-Kady, Reduction in the thermal conductivity of single crystalline silicon by phononic crystal patterning. *Nano Lett.* **11**, 107–112 (2011).
15. S. Alaie, D. F. Goettler, M. Su, Z. C. Leseman, C. M. Reinke, I. El-Kady, Thermal transport in phononic crystals and the observation of coherent phonon scattering at room temperature. *Nat. Commun.* **6**, 7228 (2015).
16. A. Jain, Y.-J. Yu, A. J. H. McGaughey, Phonon transport in periodic silicon nanoporous films with feature sizes greater than 100 nm. *Phys. Rev. B Condens. Matter Mater. Phys.* **87**, 195301 (2013).
17. A. J. Minnich, Advances in the measurement and computation of thermal phonon transport. *J. Phys. Condens. Matter* **27**, 53202 (2015).
18. N. Zen, T. A. Puurtinen, T. J. Isotalo, S. Chaudhuri, I. J. Maasilta, Engineering thermal conductance using a two-dimensional phononic crystal. *Nat. Commun.* **5**, 3435 (2014).
19. R. Anufriev, M. Nomura, Reduction of thermal conductance by coherent phonon scattering in two-dimensional phononic crystals of different lattice types. *Phys. Rev. B* **93**, 045410 (2016).
20. B. L. Davis, M. I. Hussein, Nanophononic metamaterial: Thermal conductivity reduction by local resonance. *Phys. Rev. Lett.* **112**, 055505 (2014).
21. H. Honarvar, M. I. Hussein, Spectral energy analysis of locally resonant nanophononic metamaterials by molecular simulations. *Phys. Rev. B* **93**, 081412 (2016).
22. R. Anufriev, M. Nomura, Heat conduction engineering in pillar-based phononic crystals. *Phys. Rev. B* **95**, 155432 (2017).
23. I. J. Maasilta, T. A. Puurtinen, Y. Tian, Z. Geng, Phononic thermal conduction engineering for bolometers: From phononic crystals to radial casimir limit. *J. Low Temp. Phys.* **184**, 211–216 (2016).
24. M. R. Wagner, B. Graczykowski, J. S. Reparaz, A. El Sachat, M. Sledzinska, F. Alzina, C. M. S. Torres, Two-dimensional phononic crystals: Disorder matters. *Nano Lett.* **16**, 5661–5668 (2016).
25. J. Lee, W. Lee, G. Wehmeyer, S. Dhuey, D. L. Olynick, S. Cabrini, C. Dames, J. J. Urban, P. Yang, Investigation of phonon coherence backscattering using silicon nanomeshes. *Nat. Commun.* **8**, 14054 (2017).
26. A. Balandin, K. L. Wang, Significant decrease of the lattice thermal conductivity due to phonon confinement in a free-standing semiconductor quantum well. *Phys. Rev. B* **58**, 1544–1549 (1998).
27. J. Zou, A. Balandin, Phonon heat conduction in a semiconductor nanowire. *J. Appl. Phys.* **89**, 2932–2938 (2001).
28. F. Kargar, B. Debnath, J.-P. Kakko, A. Säynätjoki, H. Lipsanen, D. L. Nika, R. K. Lake, A. A. Balandin, Direct observation of confined acoustic phonon polarization branches in free-standing semiconductor nanowires. *Nat. Commun.* **7**, 13400 (2016).
29. F. Kargar, S. Ramirez, B. Debnath, H. Malekpour, R. K. Lake, A. A. Balandin, Acoustic phonon spectrum and thermal transport in nanoporous alumina arrays. *Appl. Phys. Lett.* **107**, 171904 (2015).
30. R. Anufriev, A. Ramiere, J. Maire, M. Nomura, Heat guiding and focusing using ballistic phonon transport in phononic nanostructures. *Nat. Commun.* **8**, 15505 (2017).
31. R. Yanagisawa, J. Maire, A. Ramiere, R. Anufriev, M. Nomura, Impact of limiting dimension on thermal conductivity of one-dimensional silicon phononic crystals. *Appl. Phys. Lett.* **110**, 133108 (2017).
32. M. Nomura, Y. Kage, J. Nakagawa, T. Hori, J. Maire, J. Shiomi, R. Anufriev, D. Moser, O. Paul, Impeded thermal transport in Si multiscale hierarchical architectures with phononic crystal nanostructures. *Phys. Rev. B* **91**, 205422 (2015).
33. J. Cuffe, O. Ristow, E. Chávez, A. Shchepetov, P.-O. Chapuis, F. Alzina, M. Hettich, M. Prunnila, J. Ahopelto, T. Dekorsy, C. M. S. Torres, Lifetimes of confined acoustic phonons in ultrathin silicon membranes. *Phys. Rev. Lett.* **110**, 095503 (2013).
34. T. J. Isotalo, Y. L. Tian, I. J. Maasilta, Fabrication and modelling of three-dimensional sub-kelvin phononic crystals. *J. Phys. Conf. Ser.* **400**, 52007 (2012).
35. X. Wang, B. Huang, Computational study of in-plane phonon transport in Si thin films. *Sci. Rep.* **4**, 6399 (2014).
36. A. Malhotra, M. Maldovan, Impact of phonon surface scattering on thermal energy distribution of Si and SiGe nanowires. *Sci. Rep.* **6**, 25818 (2016).
37. A. M. Marconnet, T. Kodama, M. Asheghi, K. E. Goodson, Phonon conduction in periodically porous silicon nanobridges. *Nanoscale Microscale Thermophys. Eng.* **16**, 199–219 (2012).
38. K. Yazawa, D. Kendig, P. E. Raad, P. L. Komarov, A. Shakouri, Understanding the thermoreflectance coefficient for high resolution thermal imaging of microelectronic devices. *Electron. Cool. Mag.* **19**, 10–14 (2013).
39. R. Anufriev, J. Maire, M. Nomura, Reduction of thermal conductivity by surface scattering of phonons in periodic silicon nanostructures. *Phys. Rev. B* **93**, 045411 (2015).
40. P. D. Desai, Thermodynamic properties of iron and silicon. *J. Phys. Chem. Ref. Data* **15**, 967–983 (1986).
41. R. Rosei, D. W. Lynch, Thermomodulation spectra of Al, Au, and Cu. *Phys. Rev. B* **5**, 3883–3894 (1972).
42. M. G. Burzo, P. L. Komarov, P. E. Raad, Minimizing the uncertainties associated with the measurement of thermal properties by the transient thermo-reflectance method. *IEEE Trans. Compon. Packag. Technol.* **28**, 39–44 (2005).
43. J. Nakagawa, Y. Kage, T. Hori, J. Shiomi, M. Nomura, Crystal structure dependent thermal conductivity in two-dimensional phononic crystal nanostructures. *Appl. Phys. Lett.* **107**, 023104 (2015).
44. R. B. Peterson, Direct simulation of phonon-mediated heat transfer in a debye crystal. *J. Heat Transfer* **116**, 815–822 (1994).
45. C. Kittel, *Introduction to Solid State Physics* (Wiley, ed. 8, 2004).
46. M. G. Holland, Analysis of lattice thermal conductivity. *Phys. Rev.* **132**, 2461–2471 (1963).
47. S. Mazumder, A. Majumdar, Monte Carlo study of phonon transport in solid thin films including dispersion and polarization. *J. Heat Transfer* **123**, 749–759 (2001).
48. D. Lacroix, K. Joulain, D. Lemonnier, Monte Carlo transient phonon transport in silicon and germanium at nanoscales. *Phys. Rev. B* **72**, 064305 (2005).
49. V. Jean, S. Fumeron, K. Termentzidis, S. Tutashkonko, D. Lacroix, Monte Carlo simulations of phonon transport in nanoporous silicon and germanium. *J. Appl. Phys.* **115**, 024304 (2014).
50. S. B. Soffer, Statistical model for the size effect in electrical conduction. *J. Appl. Phys.* **38**, 1710–1715 (1967).
51. A. A. Maznev, Boundary scattering of phonons: Specularity of a randomly rough surface in the small-perturbation limit. *Phys. Rev. B* **91**, 134306 (2015).
52. M. N. Luckyanova, J. A. Johnson, A. A. Maznev, J. Garg, A. Jandl, M. T. Bulsara, E. A. Fitzgerald, K. A. Nelson, G. Chen, Anisotropy of the thermal conductivity in GaAs/AlAs superlattices. *Nano Lett.* **13**, 3973–3977 (2013).

Acknowledgments: We thank J. Tatebayashi for his help with SEM observations and K. Hirakawa, H. Han, and J. Shiomi for fruitful discussions. **Funding:** We acknowledge the support of the Project for Developing Innovation Systems of the Ministry of Education, Culture, Sports, Science and Technology (MEXT), Japan; Japan Society for the Promotion of Science (JSPS) KAKENHI (grants 25709090, 15H05869, and 15K13270); and Japan Science and Technology Agency PRESTO program (grant JPMJPR15R4). R.A. and A.R. thank the JSPS fellowship program for financial support. **Author contributions:** J.M. and R.Y. designed and fabricated the samples. J.M. performed the measurements and contributed to writing the paper. R.A. developed the cutoff frequency model and wrote the paper. A.R. performed the Monte Carlo simulations. S.V. made a major effort in the theoretical understanding of the results. M.N. conceived and supervised the entirety of the work. All authors contributed to the analysis and discussion of the results. **Competing interests:** The authors declare that they have no competing interests. **Data and materials availability:** All data needed to evaluate the conclusions in the paper are present in the paper and/or the Supplementary Materials. Additional data related to this paper may be requested from the authors. Correspondence and requests for materials should be addressed to M.N. (nomura@iis.u-tokyo.ac.jp) and J.M. (jmaire@iis.u-tokyo.ac.jp).

Submitted 3 January 2017
Accepted 29 June 2017
Published 4 August 2017
10.1126/sciadv.1700027

Citation: J. Maire, R. Anufriev, R. Yanagisawa, A. Ramiere, S. Volz, M. Nomura, Heat conduction tuning by wave nature of phonons. *Sci. Adv.* **3**, e1700027 (2017).

Heat conduction tuning by wave nature of phonons

Jeremie Maire, Roman Anufriev, Ryoto Yanagisawa, Aymeric Ramiere, Sebastian Volz and Masahiro Nomura

Sci Adv **3** (8), e1700027.
DOI: 10.1126/sciadv.1700027